Effect of a magnetospheric compression on Jovian radio emissions: in situ case study using Juno data

Corentin Louis[1]

[1]Affiliation not available

September 4, 2023

Effect of a magnetospheric compression on Jovian radio emissions: in situ case study using Juno data

C. K. Louis[1,2], C. M. Jackman[1], G. Hospodarsky[3], A. O'Kane Hackett[1,4], E. Devon-Hurley[1,4], P. Zarka[2,5], W. S. Kurth[3], R. W. Ebert[6,7], D. M. Weigt[1,8], A. R. Fogg[1], J. E. Waters[9], S. C. McEntee[1,4], J. E. P. Connerney[10], P. Louarn[11], S. Levin[12], S. J. Bolton[6]

[1]School of Cosmic Physics, DIAS Dunsink Observatory, Dublin Institute for Advanced Studies, Dublin 15, Ireland
[2]Observatoire Radioastronomique de Nançay, Observatoire de Paris, Université PSL, CNRS, University Orléans, Nancay, France
[3]Department of Physics and Astronomy, University of Iowa, Iowa City, Iowa, USA
[4]School of Physics, Trinity College Dublin, Dublin, Ireland
[5]LESIA, Observatoire de Paris, PSL Research University, CNRS, Sorbonne Université, UPMC University Paris 06, University Paris Diderot, Sorbonne Paris Cité, Meudon, France
[6]Southwest Research Institute, San Antonio, Texas, USA
[7]Department of Physics and Astronomy, University of Texas at San Antonio, San Antonio, Texas, USA
[8]Department of Computer Science, Aalto University, Aalto, Finland
[9]Department of Physics and Astronomy, University of Southampton, Highfield Campus, Southampton, SO17 1BJ, UK
[10]Space Research Corporation, Annapolis, MD
[11]IRAP, Université de Toulouse, CNRS, CNES, UPS, Toulouse, France
[12]Jet Propulsion Laboratory, Pasadena, California, USA

Key Points:

- This paper provides a list of the Jovian magnetosphere boundary crossings by the Juno spacecraft from June 2016 to August 2022.
- Jovian magnetospheric compressions lead to increased bKOM radio emissions (immediately) and DAM on the dusk sector (more than one rotation later).
- nKOM radio emission appears later during relaxation phase of the compression.

Corresponding author: Corentin Kenelm Louis, `corentin.louis@dias.ie`

Abstract

During its polar orbits around Jupiter, Juno often crosses the boundaries of the Jovian magnetosphere (namely the magnetopause and bow shock). From the boundary locations, the upstream solar wind dynamic pressure can be inferred, which in turn illustrates the state of compression or relaxation of the system. The aim of this study is to examine Jovian radio emissions during magnetospheric compressions, in order to determine the relationship between the solar wind and Jovian radio emissions. In this paper, we give a complete list of bow shock and magnetopause crossings (from June 2016 to August 2022), and the associated solar wind dynamic pressure and standoff distances inferred from Joy et al. (2002). We then select two sets of magnetopause crossings with moderate to strong compression of the magnetosphere for two case studies of the response of the Jovian radio emissions. We confirm that magnetospheric compressions lead to the activation of new radio sources. Newly-activated broadband kilometric emissions are observed almost simultaneously with compression of the magnetosphere, with sources covering a large range of longitudes. Decametric emission sources are seen to be activated more than one rotation later only at specific longitudes and dusk local times. Finally, the activation of narrowband kilometric radiation is not observed until the magnetosphere is in its expansion phase.

Plain Language Summary

1 Introduction

Planetary studies often face the challenge of interpreting *in situ* spacecraft observations without the benefit of an upstream monitor revealing the prevailing conditions in the interplanetary medium. This is particularly true of the outer planets. Radio emissions provide a direct probe of the site of particle acceleration and have potential to be used as a proxy for magnetospheric dynamics (see e.g., Cecconi et al. (2022) for Saturn; Fogg et al. (2022) for Earth). At Jupiter, the radio spectrum is composed of at least six components, from low-frequency emissions, such as quasi-periodic (QP) bursts or trapped continuum radiation (from a few kHz to 10s of kHz), up to decametric (DAM) emissions ranging from a few MHz to 40 MHz (Gurnett & Scarf, 1983; Zarka, 1998; C. K. Louis et al., 2021a).

In this study, we focus on three types of radio emissions observable with Juno: narrowband kilometric (nKOM), broadband kilometric (bKOM) and auroral DAM emissions (i.e., not induced by Galilean moons). The nKOM is attributed to a mode conversion mechanism producing emissions inside Io's torus at or near the local electron plasma frequency (Barbosa, 1982; Gurnett & Scarf, 1983; Jones, 1988; Ronnmark, 1992). The last two components (bKOM and DAM) are auroral emissions, produced by the cyclotron maser instability (CMI), near the local electron cyclotron frequency. The sources of these emissions are located on magnetic field lines of magnetic apex (M-Shell) between 10 and 60 (unitless distance of the magnetic field line at the magnetic equator normalized to Jovian radius 71492 km). These emissions are very anisotropic and beamed along the edges of a hollow cone with an opening of $\sim 75^\circ \pm 5^\circ$ to $\sim 90^\circ$ with respect to the local magnetic field lines (Ladreiter et al., 1994; Zarka, 1998; Treumann, 2006; Louarn et al., 2017, 2018; Imai et al., 2019; C. K. Louis, Prangé, et al., 2019).

The relation of the different components of Jupiter's radio emissions to both internal and external drivers is complex, as shown by several previous studies. These studies show a relationship between some of the components and external (solar wind) or internal (rotation, magnetic reconfiguration) drivers. Recently, Zarka et al. (2021) have re-analyzed data from Cassinis flyby of Jupiter, and found that hectometric (HOM) and DAM emissions are dominantly rotation-modulated (i.e. emitted from lighthouse-like sources fixed in Jovian longitude), whereas bKOM is modulated more strongly by the solar wind

than by the rotation (i.e. emitted from sources more active within a given Local Time sector). This last study extends earlier results by Zarka and Genova (1983); Genova et al. (1987); Imai et al. (2008, 2011). Louarn et al. (1998), using Galileo radio observations, have shown a sudden onset, and increased intensity (up to 2×10^{-7} V.m^{-1}.Hz$^{-1/2}$ at 5 MHz) of bKOM and DAM radio emissions, as well as the activation of new nKOM radio emissions, during periods of magnetospheric disturbance. They postulated large-scale energetic events as reconfigurations of the magnetosphere and plasmasheet somewhat analogous to terrestrial substorms. The results obtained by Echer et al. (2010), using Ulysses spacecraft data during the distant Jupiter encounter and Nançay Decameter Array (NDA) data, show that non-Io DAM radio emissions occur during intervals of enhanced solar wind dynamic pressure, but without any direct correlation between the emission duration or power versus the solar wind pressure or the interplanetary shock Mach number. Using 50 days of observations from Cassini and Galileo, Gurnett et al. (2002) showed that HOM emissions were triggered by the arrival of interplanetary shocks at Jupiter. Hess et al. (2012, 2014) have also shown that an increase of the solar wind pressure affects the non-Io-DAM radio emissions, using ground-based radio measurements (Hess et al., 2012) and Cassini and Galileo radio and magnetic measurements (Hess et al., 2014). These two studies have compared the type of shocks with the region of source activation. There are two type of shocks (Kilpua et al., 2015): fast forward shocks (FFS) and fast reverse shocks (FRS). These shocks are driven by solar coronal mass ejections (CME) or corotating interaction regions (CIR). The sudden explosion of a CME, at a higher velocity than the ambient solar wind, usually drives a FFS. As this fast CME expands into the solar system and overtakes the slower background solar wind, a compressed interaction region is usually formed, which is delimited by FFS on one side and FRS on the other side (Smith & Wolfe, 1976; Tsurutani et al., 2006). A FFS is characterized by a sharp or discontinuous increase of the solar wind velocity, density, temperature and magnetic field amplitude. A FRS is characterized by an increase of the solar wind velocity, but a decrease of the solar wind temperature, density and magnetic field amplitude. Both Hess et al. (2012, 2014) studies have shown that FFS trigger mostly dusk emissions, whereas FRS trigger both dawn and dusk emissions, with a time delay depending on the strength/direction of the interplanetary magnetic field (IMF). All the shock-triggered radio sources were found to sub-corotate (i.e. rotating slower than the rotation period of Jupiter) with a rate ranging from 50% to 80% depending on the intensity of the IMF. These rates could respectively correspond to the extended and compressed states of the Jovian magnetosphere.

The above cited studies relied on sparse datasets (flybys or remote measurements) but the once-in-a-generation Juno dataset gives the opportunity for longer-term monitoring of the Jovian system and its radio response. In particular, the apojoves early in the mission, which took Juno out to radial distances of ~ 110 R_J on the dawn side, place the spacecraft near the nominal magnetopause and bow shock locations, and afford the opportunity to sample snippets of in situ solar wind, as well as to determine the positions of the magnetospheric boundaries at various points in time. All the while, the Juno radio instrument is constantly monitoring the Jovian radio spectrum. In this study we utilise this unique dataset to explore the connection between the solar wind and Jupiter's radio emissions by presenting the first case study of its kind.

Section 2 describes the datasets and processing methodology. Section 3 presents case studies of the Jovian radio emission response to two moderate to strong magnetospheric compressions inferred from multiple magnetopause crossings while Juno is on the outbound leg of its trajectory. Finally in Section 4, we summarise and discuss the results of this study and present the perspectives.

2 Methodology

Since July 2016, Juno has been in orbit around Jupiter, making a polar orbit every 53 days during its prime mission. Since the Ganymede flyby in June 2021, the orbits have been shortened to 43 days, before being reduced to 38 days in September 2022 with the Europa flyby. During its first 44 orbits, with an apojove of up to $\sim$ 110 R_J, Juno crossed the boundaries of the magnetosphere several times (Hospodarsky et al., 2017; Ranquist et al., 2019; Montgomery et al., 2022; Collier et al., 2020), as shown in Figure 1 projected into the equatorial plane. Figure 1a displays the magnetopause crossings while Figure 1b displays the bow shock crossings. In both of these panels are drawn the 10th and 90th quantile position of the magnetopause and bow shock, respectively, based on the Joy et al. (2002) model. Note that this model was built on crossings from Ulysses, Voyager and Galileo, and thus may not be representative of all local times (especially the previously poorly explored dusk flank) or high-latitudes. The coordinate system used in this figure is the Juno-de-Spun-Sun (JSS), as this is the coordinate system used in the Joy et al. (2002) model. In this system, X points towards the Sun, Z is aligned with the Jovian spin axis, and Y closes the right-handed system (positive towards dusk). A 3D projection plot (in the Jupiter-Sun-Orbit (JSO) coordinate system) of the Jovian magnetosphere boundary crossings is shown in Figure S1 in Supporting Information (SI). In the JSO system, X is aligned with the Jupiter-Sun vector, Y indicates the Sun's motion in Jupiter frame, and Z closes the system.

In this study, the boundary crossings displayed Figure 1 were determined using the radio measurements of the low frequency receiver of the Juno/Waves instrument (Kurth et al., 2017), and the magnetic field measurements of the Juno/MAG instrument using the Fluxgate Magnetometer measurements (Connerney et al., 2017), following the work done by Hospodarsky et al. (2017). Three examples are shown in Figure 2, with Juno/Waves data (using C. K. Louis et al., 2021a, 2021b, estimated flux density data set) displayed in the top panels, and Juno/MAG data (in spherical JSO coordinates system) in the bottom panels. The "out" crossings (black dashed lines) correspond to a boundary moving towards Jupiter, e.g., Figure 2a,d, Juno crosses the bow shock going from the magnetosheath to the solar wind. The "in" crossings (grey shaded lines) define a boundary moving away from Jupiter, e.g., Juno crosses the bow shock, leaving the solar wind to enter the magnetosheath.

The bow shock is a discontinuity formed when the supersonic solar wind is slowed to subsonic by interaction with the Jovian magnetic obstacle. A bow shock crossing is detected from the change in magnetic field amplitude and in the level of field fluctuations in the Juno/MAG data between the solar wind and the magnetosheath (Figure 2d). In the Juno/Waves measurements (Figure 2a) one can observe (i) an intense and broadband signal at the crossing and (ii) Langmuir waves when Juno is inside the solar wind, visible here at $\sim$ 10 kHz, which are produced by solar electrons reflected back into the solar wind from the shock boundary (Scarf et al., 1971; Filbert & Kellogg, 1979).

The position of the magnetopause is determined by the balance between the solar wind dynamic pressure and the plasma pressure in the outer magnetosphere (Mauk et al., 2004). A magnetopause crossing is detected by the appearance/disappearance in the Juno/Waves data (see Figure 2b) of the trapped continuum radiation, usually observed between 0.5 kHz and 2 kHz. This signal is only seen when the observer is inside Jupiter's magnetosphere, in this example before the black-dashed line at $\sim$ 2017-06-18T09:00, and after the grey-shaded line at $\sim$ 2017-06-19T03:00. This trapped continuum radiation propagates at a frequency lower than the plasma frequency inside the magnetosheath and therefore can not propagate into the magnetosheath (hence the name "trapped"). Juno/MAG measurements of the magnetic field amplitude (Figure 2e) also show a change as Juno crosses the magnetopause, passing from the magnetosphere into the magnetosheath (see, e.g., black-dashed line at $\sim$ 2017-06-18T09:00), with a decrease in magnetic field total amplitude $|B|$ and a much more disturbed signal than in the magnetosphere.

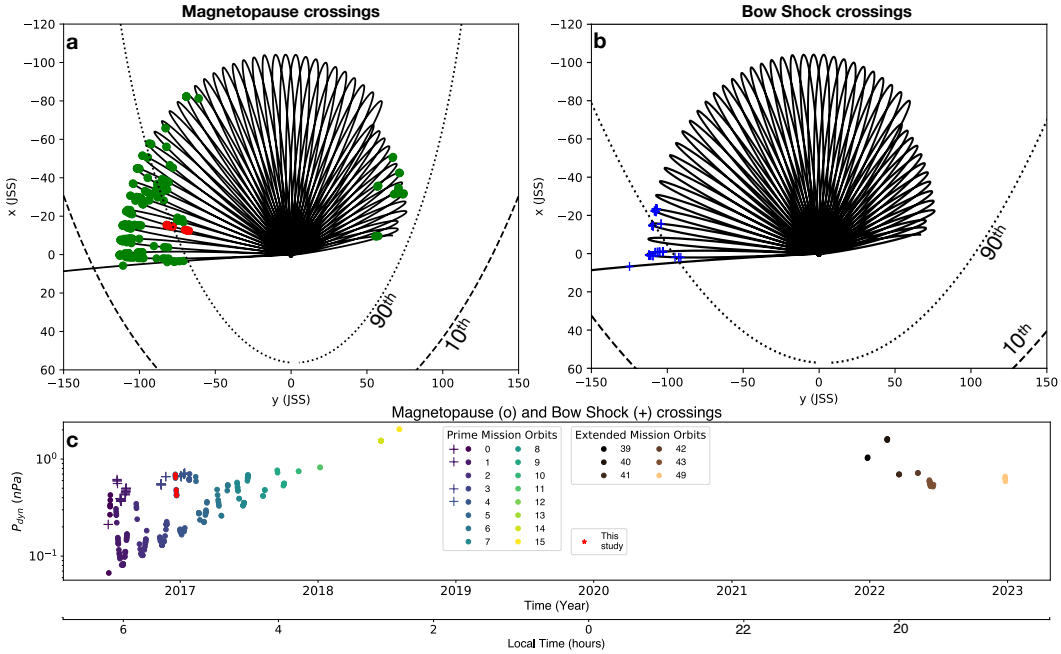

Figure 1. Projection of the Juno trajectory into the equatorial plane, with the (a) magnetopause and (b) bow-shock crossings overplotted. The magnetopause crossings studied in this article are highlighted in red in panel (a). The coordinate system used here is the Jupiter-de-Spun-Sun (JSS). In this system, X points towards the Sun, Z is aligned with the Jovian spin axis, and Y closes the right-handed system (positive towards dusk). In panel (a) the dashed line represents the 10th quantile position of the magnetopause (0.03 nPa), the dotted line its 90th quantile position (0.518 nPa). In panel (b) these same lines represent the 10th (0.063 nPa) and 90th (0.579 nPa) quantile positions of the bow shock (values from Joy et al., 2002). Panel (c) displays the solar wind dynamic pressure P_{dyn} values inferred from Joy et al. (2002), for each crossing ("+": magnetopause; "o": bow shock), as a function of time and Local Time (1200: direction of the Sun; 0000: opposition to the Sun). The colour code corresponds to the orbit number. The cases studied in this article are highlighted in red.

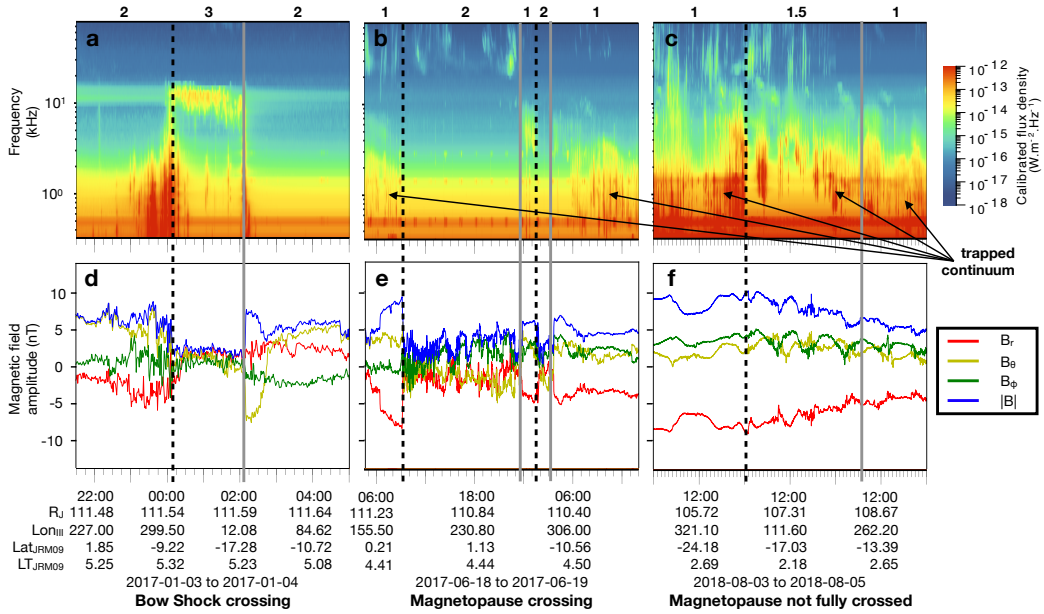

Figure 2. Examples of magnetospheric boundary crossings. Top panels (a-c) display Juno/Waves measurements (using C. K. Louis et al., 2021a, 2021b, estimated flux density data set), while bottom panels (d-f) display Juno/MAG measurements in spherical JSO coordinates. Outbound crossings (boundary moving towards Jupiter) are highlighted by the black-dashed lines, while inbound crossings (boundary moving away from Jupiter) are highlighted by the grey-shaded lines. (left (a,d)) Bow shock crossings; (middle (b,e)) Magnetopause crossings; (right (c,f)) Example where the Juno spacecraft partially crossed the magnetopause without ever actually passing from the magnetosphere to the magnetosheath (i.e. moved around the border). The numbers above the Waves data indicate the region where Juno is located: (1): Magnetosphere, (2) Magnetosheath, (3) Solar Wind, (1.5): "in" the magnetopause boundary.

In some observations (see Figure 2c, between black-dashed and grey-shaded lines), low and high cut-off frequencies of the trapped continuum increase. Before $\sim$ 2018-08-04T00:00 (black-dashed line) and after $\sim$ 2018-08-05T07:00 (grey-shaded line), the trapped-continuum radiation is visible between $\sim$ 0.3 kHz and $\sim$ 4 kHz. In-between, the trapped-continuum radiation is no longer visible at low frequency, but is shifted to higher frequencies (between $\sim$ 0.6 and $\sim$ 8 kHz) and is very bursty. The high frequency part never completely disappears, and no drastic change in magnetic field components (Figure 2f) is observed, although they are more disturbed than in the magnetosphere, but less than in the magnetosheath. In the observation shown in Figures 2c,f, Juno is on the outbound part of its trajectory and is therefore moving away from Jupiter. We interpret these observations as the movement of the magnetopause towards Juno at first (increase of low and high cut-off frequencies, see black-dashed line). Subsequently, the magnetopause stops moving towards Jupiter, and Juno never completely crosses the magnetopause to end up in the magnetosheath (between black-dashed and grey-shaded lines). Juno is however close enough to the magnetopause , or even in the boundary layer (Went et al., 2011), to observe an increase of the low-frequency cutoff of the trapped continuum by the increasing density when approaching the boundary. Finally, the magnetopause is moving away from Jupiter (faster than Juno's velocity), and high and low cut-off frequencies decrease (Juno is again completely in the magnetosphere).

From the boundary positions, we can infer the solar wind dynamic pressure P_{dyn} using the Joy et al. (2002) model, by solving their second order polynomial equation (equation 1 of Joy et al., 2002). From this, we can determine if the crossings of the magnetospheric boundaries are due to compressions of the magnetosphere, by comparing the inferred P_{dyn} values to either Joy et al. (2002) quantile values, or observed solar wind P_{dyn} distributions upstream of Jupiter (Jackman & Arridge, 2011). One should note that the P_{dyn} value determined using Juno's position is not absolute, but a lower limit of the dynamic pressure. Although Juno is outbound, we cannot directly infer how far the magnetopause boundary is pushed back towards Jupiter.

Figure 1c displays the inferred P_{dyn} for all crossings ("+": magnetopause; "o": bow shock) as a function of time and Local Time. Note that there is a trend of increasing P_{dyn} values with time and decreasing Local Time. This is due to the procession of orbits, taking Juno more and more towards the night side of the magnetosphere (midnight Local Time), and thus deep into the magnetotail. This means that the magnetosphere has to be more compressed for Juno to cross the magnetospheric boundaries from this location. The bow shock is even further out again and thus Juno did not encounter the dawn side bow shock after the first few Juno orbits.

In the absence of an upstream monitor, we can compare these inferred P_{dyn} values with those provided by solar wind propagation models (e.g., Tao et al., 2005). For this, we must take into account any uncertainty on the propagation model values due to angle from opposition where predictions are most reliable. From this propagation model, we can also infer the type of shock (FFS or FRS) that compresses the magnetosphere as discussed in Section 1.

The full list of magnetopause and bow shock crossings (from 2016-06-24 to 2022-07-26, i.e. up to orbit 41) are available in Table S1 and S2 in Supplementary Information (SI), along with the position of Juno (in cartesian JSS –mandatory to use Joy et al. (2002) model– and cartesian and spherical International Astronomical Union (IAU) System III (SIII) coordinates system), the inferred solar wind dynamic pressure and the position of the magnetosphere standoff distances (bow shock and magnetopause) inferred from the Joy et al. (2002) model (C. K. Louis et al., 2022e). Figure S2 displays statistical distributions based on the magnetosphere boundary crossings (Local Time, Solar Wind dynamic pressure, magnetopause and bow shock positions).

We next investigate the response of bKOM and DAM emissions to magnetospheric compression in a case study. For that, we use the C. K. Louis et al. (2021a) dataset (C. K. Louis et al., 2021b) and catalogue of the radio emissions (C. K. Louis et al., 2021c). This catalogue contains the Jovian radio emissions identified in the Juno/Waves observations, only from 2016-04-09 to 2019-06-24 (e.g. up to the 21st apojove of Juno). The radio components were visually identified according to their time-frequency morphology and then manually encircled by contours and labeled, using a dedicated program that records the coordinates of the contours and the label of each emission patch (C. Louis et al., 2022a; C. K. Louis et al., 2022b). While nKOM patches can be identified individually (fuzzy patches of emission elongated in time), the bKOM and DAM components have not been explicitly catalogued because they are the most frequent emissions in their respective frequency range. They can be selected and studied by excluding all other components and restricting to the adequate frequency range. For example, excluding nKOM in the range 20-140 kHz allows one to select the bKOM component only. In the [3.5-40.5] MHz frequency range, only decametric emissions induced by the Galilean moons Io, Europa and Ganymede have been labelled (based on C. K. Louis, Hess, et al. (2019) simulations of those radio emissions, see C. K. Louis et al. (2020) for more details). Therefore, by excluding them, only auroral DAM emissions remain in this range. Given that HOM emissions can extend up to a few MHz, the highest part of the hectometric emission could be present in this range, but would only represent a minority of the emissions observed.

For the case studies described in Section 3, we decided to select the magnetopause crossings that took place between 2016-12-19 and 2016-12-23, highlighted in red in Figure 1. This choice is based on three factors: (i) in 2016-2017, the Jovian Auroral Distributions Experiment (JADE, McComas et al., 2017) was not activated during excursions into the solar wind, excluding *in situ* plasma information, and thus a direct measurement of P_{dyn}. Therefore, we decided to choose among one of the (more numerous) magnetopause crossing cases; (ii) the case chosen had to be within the time interval covered by the catalogue of C. K. Louis et al. (2021a, i.e. between 2016-04-09 and 2019-06-24); (iii) in order to avoid any bias related to an extremely exceptional case, we did not select the case with the highest P_{dyn} value (second half of 2018, orbit 15).

The time interval chosen presents two main advantages. (i) There are two sets of crossings in a row. The P_{dyn} value determined for the first crossing (2016-12-19T01:50) is 0.70 nPa. The dynamic pressure associated with the second set of crossings (2016-12-21T08:48) is 0.48 nPa. The distribution of P_{dyn} at Jupiter published by Jackman and Arridge (2011, see their Figure 4b) reveals a peak at 0.05 nPa and a maximum slightly above 1 nPa. The 0.48 and 0.70 values therefore lie towards the tail of this distribution. Moreover, these inferred values are close to the 90th quantile value (0.518 nPa) of the magnetopause position given by Joy et al. (2002). Therefore, these two sets of magnetopause crossings correspond to a strong and a moderate compression. (ii) Based on Figure 1c (red points) the P_{dyn} values associated with these magnetopause crossings are well above the "trend", and therefore correspond to the strongest compressions during orbit 4. Recall that this "trend" is due to the procession of Juno's orbit, taking the spacecraft deep into the magnetotail, implying that the magnetosphere needs to be more compressed for Juno to cross the magnetospheric boundaries.

3 Jovian auroral radio emission response to compressions of the magnetosphere

3.1 Determination of the compression

Figure 3 displays Juno measurements during magnetopause crossings for a 7-day interval from 2016-12-17T00:00 to 2016-12-24T04:15. Black-dashed lines show when Juno crossed the magnetopause from the magnetosphere to the magnetosheath (outbound crossings), while grey-shaded lines show inbound crossings. Figures 3a,b display Juno/Waves

Figure 3. (a-c) Juno Waves and MAG measurements during a series of magnetopause crossings. Panels (a) and (b) show Juno Waves frequency-time spectrograms covering two di erent frequency ranges (from 3.5 to 40.5 MHz and between 3 kHz and 140 kHz, respectively), with the black polygons in the top panel denoting the radio emissions induced by the interaction between Jupiter and its moons (e.g. Io, Europa or Ganymede, based on C. K. Louis et al., 2021c). Panel (c) shows the three components of magnetic eld (in JSO spherical coordinates system, red, yellow and green lines) and total eld strength (blue). The black line displays the Kivelson and Khurana (2002); Khurana et al. (2004) magnetic eld variation t. Panels (d-f) display time series of integrated ux density (normalized at 1 Astronomical Unit (AU), 15 sec time resolution) for (d) the auroral decametric (DAM, in the 3 :5-40.5 MHz range) not induced by the interaction between Jupiter and its moons (i.e. all the non-labelled emissions), (e) broadband kilometric (bKOM, in the 20-140 kHz range) and (f) narrowband kilometric (nKOM, in the 40-140 kHz range) radio emissions.
The black-dashed lines represent the outbound magnetopause crossings (from the magnetosphere to the magnetosheath) while the grey-shaded lines represent the inbound magnetopause crossings (from the magnetosheath to the magnetosphere). The red-dashed line represents the time when Juno starts to measure magnetic uctuations and $|B| > |B_{lobe}|$ (panel c), and an increase in the low and high cut-o frequencies of the trapped-continuum radiation (panel b).
The numbers above the Waves data indicate the region where Juno is located: (1): Magnetosphere, (2) Magnetosheath, (1.5): \in" the magnetopause boundary.

10.3389/fspas.2022.800279

Collier, M. R., Gruesbeck, J. R., Connerney, J. E. P., Joy, S. P., Hospodarsky, G. B., Roberts, A., ... Roelof, E. C. (2020, September). A K-Means Clustering Analysis of the Jovian and Terrestrial Magnetopauses: A Technique to Classify Global Magnetospheric Behavior. *Journal of Geophysical Research (Planets)*, *125*(9), e06366. doi: 10.1029/2019JE006366

Connerney, J. E. P. (2017). *Juno MAG CALIBRATED DATA J V1.0, JNO-J-3-FGM-CAL-V1.0 [dataset].* doi: 10.17189/1519711

Connerney, J. E. P., Benn, M., Bjarno, J. B., Denver, T., Espley, J., Jorgensen, J. L., ... Smith, E. J. (2017, November). The Juno Magnetic Field Investigation. *Space Science Reviews*, *213*, 39-138. doi: 10.1007/s11214-017-0334-z

Echer, E., Zarka, P., Gonzalez, W. D., Morioka, A., & Denis, L. (2010, September). Solar wind effects on Jupiter non-Io DAM emissions during Ulysses distant encounter (2003-2004). *Astronomy & Astrophysics*, *519*, A84. doi: 10.1051/0004-6361/200913305

Faden, J. B., Weigel, R. S., Merka, J., & W., F. R. H. (2010, June). Autoplot: a browser for scientific data on the web. *Earth. Sci. Inform.*, *3*, 41-49. doi: 10.1007/s12145-010-0049-0

Filbert, P. C., & Kellogg, P. J. (1979, April). Electrostatic noise at the plasma frequency beyond the earth's bow shock. *Journal of Geophysical Resarch*, *84*(A4), 1369-1381. doi: 10.1029/JA084iA04p01369

Fogg, A. R., Jackman, C. M., Waters, J. E., Bonnin, X., Lamy, L., Cecconi, B., ... Louis, C. K. (2022, May). Wind/WAVES Observations of Auroral Kilometric Radiation: Automated Burst Detection and Terrestrial Solar Wind - Magnetosphere Coupling Effects. *Journal of Geophysical Research (Space Physics)*, *127*(5), e30209. doi: 10.1029/2021JA030209

Génot, V., Budnik, E., Jacquey, C., Bouchemit, M., Renard, B., Dufourg, N., ... Cabrolie, F. (2021, July). Automated Multi-Dataset Analysis (AMDA): An on-line database and analysis tool for heliospheric and planetary plasma data. *Planetary and Space Sciences*, *201*, 105214. doi: 10.1016/j.pss.2021.105214

Genova, F., Zarka, P., & Barrow, C. H. (1987, August). Voyager and Nancay observations of the Jovian radio-emission at different frequencies - Solar wind effect and source extent. *Astronomy & Astrophysics*, *182*, 159-162.

Gurnett, D. A., Kurth, W. S., Hospodarsky, G. B., Persoon, A. M., Zarka, P., Lecacheux, A., ... Dougherty, M. K. (2002, February). Control of Jupiter's radio emission and aurorae by the solar wind. *Nature*, *415*, 985-987. doi: 10.1038/415985a

Gurnett, D. A., & Scarf, F. L. (1983). Physics of the Jovian magnetosphere. 8. Plasma waves in the Jovian magnetosphere. In *Physics of the jovian magnetosphere* (p. 285-316).

Hess, S. L. G., Echer, E., & Zarka, P. (2012, September). Solar wind pressure effects on Jupiter decametric radio emissions independent of Io. *Planetary Space Science*, *70*, 114-125. doi: 10.1016/j.pss.2012.05.011

Hess, S. L. G., Echer, E., Zarka, P., Lamy, L., & Delamere, P. A. (2014, September). Multi-instrument study of the Jovian radio emissions triggered by solar wind shocks and inferred magnetospheric subcorotation rates. *Planetary Space Science*, *99*, 136-148. doi: 10.1016/j.pss.2014.05.015

Hospodarsky, G. B., Kurth, W. S., Bolton, S. J., Allegrini, F., Clark, G. B., Connerney, J. E. P., ... Valek, P. W. (2017, May). Jovian bow shock and magnetopause encounters by the Juno spacecraft. *Geophysical Research Letters*, *44*(10), 4506-4512. doi: 10.1002/2017GL073177

Imai, M., Greathouse, T. K., Kurth, W. S., Gladstone, G. R., Louis, C. K., Zarka, P., ... Connerney, J. E. P. (2019, Jan). Probing Jovian Broadband Kilometric Radio Sources Tied to the Ultraviolet Main Auroral Oval With Juno. *Geophysical Research Letters*, *46*(2), 571-579. doi: 10.1029/2018GL081227

Imai, M., Imai, K., Higgins, C. A., & Thieman, J. R. (2008, September). Angular beaming model of Jupiter's decametric radio emissions based on Cassini RPWS data analysis. Geophysical Research Letters, 35(17), L17103. doi: 10.1029/2008GL034987

Imai, M., Imai, K., Higgins, C. A., & Thieman, J. R. (2011, December). Comparison between Cassini and Voyager observations of Jupiter's decametric and hectometric radio emissions. Journal of Geophysical Research (Space Physics), 116(A12), A12233. doi: 10.1029/2011JA016456

Imai, M., Kurth, W. S., Hospodarsky, G. B., Bolton, S. J., Connerney, J. E. P., & Levin, S. M. (2017, May). Statistical study of latitudinal beaming of Jupiter's decametric radio emissions using Juno. Geophysical Research Letters, 44(10), 4584-4590. doi: 10.1002/2017GL073148

Jackman, C. M., & Arridge, C. S. (2011, December). Solar Cycle E ects on the Dynamics of Jupiter's and Saturn's Magnetospheres. Solar Physics, 274(1-2), 481-502. doi: 10.1007/s11207-011-9748-z

Jackman, C. M., Arridge, C. S., Slavin, J. A., Milan, S. E., Lamy, L., Dougherty, M. K., & Coates, A. J. (2010, October). In situ observations of the e ect of a solar wind compression on Saturn's magnetotail. Journal of Geophysical Research (Space Physics), 115(A10), A10240. doi: 10.1029/2010JA015312

Jones, D. (1988, January). Planetary radio emissions from low magnetic latitudes - Observations and theories. In Planetary radio emissions ii (p. 245-281).

Joy, S. P., Kivelson, M. G., Walker, R. J., Khurana, K. K., Russell, C. T., & Ogino, T. (2002, October). Probabilistic models of the Jovian magnetopause and bow shock locations. Journal of Geophysical Research (Space Physics), 107(A10), 1309. doi: 10.1029/2001JA009146

Khurana, K. K., Kivelson, M. G., Vasyliunas, V. M., Krupp, N., Woch, J., Lagg, A., . . . Kurth, W. S. (2004). The con guration of Jupiter's magnetosphere. In F. Bagenal, T. E. Dowling, & W. B. McKinnon (Eds.), Jupiter. the planet, satellites and magnetosphere (Vol. 1, p. 593-616).

Kilpua, E. K. J., Lumme, E., Andreeova, K., Isavnin, A., & Koskinen, H. E. J. (2015). Properties and drivers of fast interplanetary shocks near the orbit of the earth (19952013). Journal of Geophysical Research: Space Physics, 120(6), 4112-4125. Retrieved from https://agupubs.onlinelibrary.wiley.com/doi/abs/10.1002/2015JA021138 doi: https://doi.org/10.1002/2015JA021138

Kivelson, M. G., & Khurana, K. K. (2002, August). Properties of the magnetic eld in the Jovian magnetotail. Journal of Geophysical Research (Space Physics), 107(A8), 1196. doi: 10.1029/2001JA000249

Kurth, W. S., Hospodarsky, G. B., Kirchner, D. L., Mokrzycki, B. T., Averkamp, T. F., Robison, W. T., . . . Zarka, P. (2017, November). The Juno Waves Investigation. Space Science Reviews, 213, 347-392. doi: 10.1007/s11214-017-0396-y

Ladreiter, H. P., Zarka, P., & Lacacheux, A. (1994, November). Direction nding study of Jovian hectometric and broadband kilometric radio emissions: Evidence for their auroral origin. Planetary Space Science, 42, 919-931. doi: 10.1016/0032-0633(94)90052-3

Lamy, L., Kenfack, G., Zarka, P., Cecconi, B., Viou, c., P., R., . . . A., C. (2021). Nanay Decameter Array (NDA) Jupiter Juno-Nanay data collection (Version 1.0) [Data set]. PADC/MASER. doi: 10.25935/PBPE-BF82

Louarn, P., Allegrini, F., McComas, D. J., Valek, P. W., Kurth, W. S., Andre, N., . . . Zink, J. L. (2017, May). Generation of the Jovian hectometric radiation: First lessons from Juno. Geophysical Research Letters, 44, 4439-4446. doi: 10.1002/2017GL072923

Louarn, P., Allegrini, F., McComas, D. J., Valek, P. W., Kurth, W. S., Andre, N., . . . Wilson, R. J. (2018, September). Observation of Electron Conics by Juno:

Implications for Radio Generation and Acceleration Processes. Geophysical Research Letters, 45(18), 9408-9416. doi: 10.1029/2018GL078973

Louarn, P., Kivelson, M. G., & Kurth, W. S. (2016, October). On the links between the radio ux and magnetodisk distortions at Jupiter. Journal of Geophysical Research (Space Physics), 121(10), 9651-9670. doi: 10.1002/2016JA023106

Louarn, P., Roux, A., Perraut, S., Kurth, W., & Gurnett, D. (1998, January). A study of the large-scale dynamics of the Jovian magnetosphere using the Galileo Plasma Wave Experiment. Geophysical Research Letters, 25(15), 2905-2908. doi: 10.1029/98GL01774

Louis, C., Jackman, C., Mangham, S., Smith, K., O'Dwyer, E., Empey, A., . . . Maloney, S. (2022a, November). The \SPectrogram Analysis and Cataloguing Environment" (SPACE) labelling tool. Frontiers in Astronomy and Space Sciences, 9, 1001166. doi: 10.3389/fspas.2022.1001166

Louis, C. K., Cecconi, B., & Loh, A. (2020). ExPRES Jovian Radio Emission Simulations Data Collection (Version 01). PADC. doi: 10.25935/KPGE-ZB59

Louis, C. K., Hess, S. L. G., Cecconi, B., Zarka, P., Lamy, L., Aicardi, S., & Loh, A. (2019, Jul). ExPRES: an Exoplanetary and Planetary Radio Emissions Simulator. Astronomy & Astrophysics, 627, A30. doi: 10.1051/0004-6361/201935161

Louis, C. K., Hospodarsky, G., Jackman, C. M., O'Kane Hackett, A., Devon-Hurley, E., Kurth, W. S., . . . Connerney, J. E. P. (2022e). Lists of magnetopause and bow shock crossings, as measured by Juno/Waves and Juno/MAG (1.0.0) [Data set]. DIAS/Zenodo. Retrieved from https://doi.org/10.5281/zenodo.6460746 doi: 10.5281/zenodo.7304516

Louis, C. K., Jackman, C. M., Mangham, S. W., Smith, K. D., O'Dwyer, E., Empey, A., . . . Maloney, S. (2022b). SPACE Labelling Tool Version 2.0.0 (v2.0.0) [Code]. Zenodo. doi: 10.5281/zenodo.6886528

Louis, C. K., Lamy, L., Zarka, P., Cecconi, B., Imai, M., Kurth, W. S., . . . Levin, S. M. (2017, September). Io-Jupiter decametric arcs observed by Juno/Waves compared to ExPRES simulations. Geophysical Research Letters, 44, 9225-9232. doi: 10.1002/2017GL073036

Louis, C. K., Prange, R., Lamy, L., Zarka, P., Imai, M., Kurth, W. S., & Connerney, J. E. P. (2019, November). Jovian Auroral Radio Sources Detected In Situ by Juno/Waves: Comparisons With Model Auroral Ovals and Simultaneous HST FUV Images. Geophysical Research Letters, 46(21), 11,606-11,614. doi: 10.1029/2019GL084799

Louis, C. K., Zarka, P., & Cecconi, B. (2021b). Juno/Waves estimated ux density Collection (Version 1.0). PADC/MASER. doi: 10.25935/6jg4-mk86

Louis, C. K., Zarka, P., Cecconi, B., & Kurth, W. S. (2021c). Catalogue of Jupiter radio emissions identi ed in the Juno/Waves observations (Version 1.0). PADC/MASER. doi: 10.25935/nhb2-wy29

Louis, C. K., Zarka, P., Dabidin, K., Lampson, P. A., Magalhães, F. P., Boudouma, A., . . . Cecconi, B. (2021a, October). Latitudinal Beaming of Jupiter's Radio Emissions From Juno/Waves Flux Density Measurements. Journal of Geophysical Research (Space Physics), 126(10), e29435. doi: 10.1029/2021JA029435

Mauk, B. H., Mitchell, D. G., McEntire, R. W., Paranicas, C. P., Roelof, E. C., Williams, D. J., . . . Lagg, A. (2004, September). Energetic ion characteristics and neutral gas interactions in Jupiter's magnetosphere. Journal of Geophysical Research (Space Physics), 109(A9), A09S12. doi: 10.1029/2003JA010270

McComas, D. J., Alexander, N., Allegrini, F., Bagenal, F., Beebe, C., Clark, G., . . . White, D. (2017, November). The Jovian Auroral Distributions Experiment (JADE) on the Juno Mission to Jupiter. Space Science Reviews, 213, 547-643. doi: 10.1007/s11214-013-9990-9

Michael, A. T., Sorathia, K. A., Merkin, V. G., Nykyri, K., Burkholder, B., Ma, X., . . . Garretson, J. (2021, October). Modeling Kelvin-Helmholtz Instability at the High-Latitude Boundary Layer in a Global Magnetosphere Simulation.

Geophysical Research Letters, 48(19), e94002. doi: 10.1029/2021GL094002
Montgomery, J., Ebert, R. W., Clark, G., Fuselier, S. A., Allegrini, F., Bagenal, F., ... Wilson, R. J. (2022, July). Investigating the Occurrence of Magnetic Reconnection at Jupiter's Dawn Magnetopause During the Juno Era. Geophysical Research Letters, 49(14), e99141. doi: 10.1029/2022GL099141
Owens, M., Lang, M., Barnard, L., Riley, P., Ben-Nun, M., Scott, C. J., ... Gonzi, S. (2020, March). A Computationally E cient, Time-Dependent Model of the Solar Wind for Use as a Surrogate to Three-Dimensional Numerical Magnetohydrodynamic Simulations. Solar Physics, 295(3), 43. doi: 10.1007/s11207-020-01605-3
Ranquist, D. A., Bagenal, F., Wilson, R. J., Hospodarsky, G., Ebert, R. W., Allegrini, F., ... Bolton, S. J. (2019, November). Survey of Jupiter's Dawn Magnetosheath Using Juno. Journal of Geophysical Research (Space Physics), 124(11), 9106-9123. doi: 10.1029/2019JA027382
Reville, V., Poirier, N., Kouloumvakos, A., Rouillard, A. P., Ferreira Pinto, R., Fargette, N., ... Scoul, C. (2023, March). HelioCast: heliospheric forecasting based on white-light observations of the solar corona. Journal of Space Weather and Space Climate, 13, 11. doi: 10.1051/swsc/2023008
Ronnmark, K. (1992, January). Conversion of Upper Hybrid waves into magnetospheric radiation. In Planetary radio emissions iii (p. 405-417).
Rouillard, A. P., Lavraud, B., Genot, V., Bouchemit, M., Dufourg, N., Plotnikov, I., ... Mays, L. (2017, November). A propagation tool to connect remote-sensing observations with in-situ measurements of heliospheric structures. Planetary and Space Science, 147, 61-77. doi: 10.1016/j.pss.2017.07.001
Scarf, F. L., Fredricks, R. W., Frank, L. A., & Neugebauer, M. (1971, January). Nonthermal electrons and high-frequency waves in the upstream solar wind, 1. Observations. Journal of Geophysical Research, 76(22), 5162. doi: 10.1029/JA076i022p05162
Smith, E. J., & Wolfe, J. H. (1976, March). Observations of interaction regions and corotating shocks between one and ve AU: Pioneers 10 and 11. Geophysical Research Letters, 3(3), 137-140. doi: 10.1029/GL003i003p00137
Tao, C., Kataoka, R., Fukunishi, H., Takahashi, Y., & Yokoyama, T. (2005, November). Magnetic eld variations in the Jovian magnetotail induced by solar wind dynamic pressure enhancements. Journal of Geophysical Research (Space Physics), 110(A11), A11208. doi: 10.1029/2004JA010959
Thomsen, M. F., Jackman, C. M., & Lamy, L. (2019, October). Solar Wind Dynamic Pressure Upstream From Saturn: Estimation From Magnetosheath Properties and Comparison With SKR. Journal of Geophysical Research (Space Physics), 124(10), 7799-7819. doi: 10.1029/2019JA026819
Treumann, R. A. (2006, August). The electron-cyclotron maser for astrophysical application. Astronomy & Astrophysicsr, 13, 229-315. doi: 10.1007/s00159-006-0001-y
Tsurutani, B. T., Gonzalez, W. D., Gonzalez, A. L. C., Guarnieri, F. L., Gopalswamy, N., Grande, M., ... Vasyliunas, V. (2006, July). Corotating solar wind streams and recurrent geomagnetic activity: A review. Journal of Geophysical Research (Space Physics), 111(A7), A07S01. doi: 10.1029/2005JA011273
Went, D. R., Kivelson, M. G., Achilleos, N., Arridge, C. S., & Dougherty, M. K. (2011, April). Outer magnetospheric structure: Jupiter and Saturn compared. Journal of Geophysical Research (Space Physics), 116(A4), A04224. doi: 10.1029/2010JA016045
Zarka, P. (1998, September). Auroral radio emissions at the outer planets: Observations and theories. Journal of Geophysics Research, 103, 20159-20194. doi: 10.1029/98JE01323
Zarka, P., & Genova, F. (1983, December). Low-frequency Jovian emission and solar wind magnetic sector structure. Nature, 306(5945), 767-768. doi: 10.1038/

306767a0

Zarka, P., Magalhães, F. P., Marques, M. S., Louis, C. K., Echer, E., Lamy, L., ... Prangé, R. (2021, October). Jupiter's Auroral Radio Emissions Observed by Cassini: Rotational Versus Solar Wind Control, and Components Identification. Journal of Geophysical Research (Space Physics), 126(10), e29780. doi: 10.1029/2021JA029780